Is spark plasma sintering suitable for the densification of continuous carbon fibre - UHTCMCs?

Is spark plasma sintering suitable for the densification of continuous carbon fibre - UHTCMCs?

Luca Zoli [a], Antonio Vinci [a], Pietro Galizia [a], Carlos F. Guitèrrez-Gonzalez [b], Sergio Rivera [b], Diletta Sciti [a, *]

[a] CNR-ISTEC, Institute of Science and Technology for Ceramics, Via Granarolo 64, I-48018 Faenza, Italy

[b] Nanoker Research S.L., Polígono de Olloniego, Parcela 22A - Nave 5, 33660 Oviedo, Principado de Asturias (Spain)

*Corresponding author: D. Sciti, diletta.sciti@istec.cnr.it, phone +39 0546 699748, fax +39 0546 46381

ABSTRACT

For the first time we show that spark plasma sintering can efficiently replace hot pressing for the densification of UHTCMCs, in the present case ZrB_2/SiC composites reinforced with continuous carbon fibres. To this purpose, the same materials were first produced by hot pressing as baseline samples and then by spark plasma sintering (SPS) to compare microstructure and basic mechanical properties. A special emphasis was given to the study of interfaces, in case of both coated and uncoated carbon fibres.

SPS allowed for faster sintering but required an adjustment of the temperature to avoid fibre degradation compared to hot pressing. With similar porosity levels, we observed a slight decrease of flexural strength (300 vs 470 MPa), and an improvement of fracture toughness (15 vs 10 MPa√m) for SPSed samples. SPS was proved to be an effective method for the consolidation of continuous fibre reinforced UHTC composites.

Keywords: spark plasma sintering; ceramic matrix composite; UHTCMC; carbon fibre; hot pressing

1. Introduction

Spark plasma sintering (SPS) is a consolidation technique for the processing of several class of materials and configurations. [1–3] The simultaneous application of electrical current and mechanical pressure allows to overcome many of the problems encountered with poorly sinterable materials [4–8]. The advantages of SPS over hot pressing for refractory ceramic bulk compounds such as Ultra-High Temperature Ceramics (UHTCs) has been proved in several publications [9–12]. With this technique it is possible to reduce the maximum temperature, holding time and/or avoid the use of sintering agents, which results in overall refinement of the microstructure and improvement of mechanical properties [13]. Recently, fast consolidation of ZrB_2-based composites reinforced with ultra-short pitch-based carbon fibres (<0.5 mm) has been obtained by SPS, with minimal or no fibre damage provided that the sintering parameters are carefully tailored[14].

This paper investigates for the first time the SPS densification of continuous carbon fibre - UHTCMCs obtained by overlapping carbon fibre preforms impregnated with ZrB_2-SiC powder mixtures. UHTCMCs are under development in the European project C^3HARME (www.c3harme.eu) and are designed to be applied in aerospace harsh environments such as thermal protection systems for hypersonic re-entry vehicles and rocket nozzles for satellite launchers [15,16]. UHTCMCs should in principle overcome the operational limits of SiC-based CMCs, due to active oxidation of SiC to $SiO_{(g)}$ at temperatures above 1600 °C and at low oxygen partial pressures [17–21]. Several processing methods are currently under investigation to combine the functionality of the UHTC phase with the damage tolerance of CMCs; one approach is based on the coating of CMCs with a layer of UHTCs [22], while other methods involve the incorporation of UHTC particles in the starting liquid precursor [19,23,24]. In all these cases the UHTC phase represent a very low volumetric fraction of the final composite [25–27]

Hot pressed continuous carbon fibre-UHTCMCs are basically constituted by a UHTC matrix well integrated with the carbon preform, and have recently shown an excellent oxidation

resistance [18], thermal shock resistance up to 1500 °C [26] and damage tolerance [28]. Further investigations have been carried out on ablation behaviour under hypersonic re-entry conditions [29] demonstrating an excellent behaviour at temperature exceeding 2500 °C.

In the present work, consolidation efficiency of C_f/ZrB_2-SiC UHTCMCs by spark plasma sintering was investigated. On the same materials, hot pressing cycles were performed as reference. Sintering parameters, microstructural features and mechanical properties were compared in order to understand advantages and drawbacks of the SPS technology. This work also includes the study of sinterability and characterization with two different types of fibres i.e.:

- pyrolytic carbon (PyC) coated PAN-based carbon fibres,
- uncoated pitch-based carbon fibres.

2. Experimental

Fabrication. The following raw materials were used:

Powders: ZrB_2 Grade B, H.C. Starck, Germany, particle size range 0.5-6 µm, impurities (wt%): 0.2 C, 1.3 O, 0.19 N, 0.1 Fe, 1.4 Hf; α-SiC (Grade UF-25, H.C. Starck, Germany, D_{50} 0.45 µm.

Fibres: PAN-derived Carbon fibres (T800HB-6000, TORAYCA, Japan), diameter 5 µm, coating: pyrolytic carbon (PyC) 0.0811 g/m (coating thickness ~0.5-1 µm); pitch-based carbon fibres (XN80-6K, Granoc, Japan), diameter 10 µm, uncoated.

A (90 vol% ZrB_2 - 10 vol% SiC) powder mixture was prepared by wet ball milling and dried. With the mixed powders, aqueous slurries were prepared according to previous studies [25]. Composites were fabricated impregnating unidirectional fibre bundles with the slurry and subsequently stacking the fibre layers, either 30 x 30 mm^2 squares or Ø = 40 mm discs, in a 0/0° configuration. The 4 materials have the following compositions, in vol% (see details in Table 1):

45% (90 %ZrB_2-10 % SiC) + 55 vol% PyC PAN-C_f, labelled as **C_SPS** or **C_HP**,

55% (90 % ZrB_2-10 % SiC) + 45 vol% Pitch-C_f, labelled as **U_SPS** or **U_HP**,

where “C” refers to coated fibres, “U” to uncoated fibres, “SPS” to spark plasma sintering ad “HP” to hot pressing.

Sintering. Hot pressing cycles were carried out on 30 x 30 mm^2 samples on the basis of previous experience [26], under vacuum (~0.2 mbar), at 1900 °C, 40 MPa, holding time of 30 min, heating rate of 25 °C/min, free cooling. The temperature behaviour was monitored by an optical pyrometer focused on the external surface of the graphite die. Since the heating rate is low and the sample highly thermally conductive we assume that temperature experienced by the sample is consistent with the value measured by the pyrometer. Spark plasma sintering cycles (SPS furnaces HPD25, FCT Systeme GMBH, Germany) on Ø = 40 mm discs were carried out under vacuum (~0.3 mbar) at 1850, 1900 °C, holding time 2-5 mm, heating rate 100 °C/min, cooling rate 450 °C/minute. The temperature was monitored with an optical pyrometer focused on the bottom of the upper graphite punch, about 5 mm away from the sample. The final pressure of 40 MPa was applied at the beginning of the cycle and released at the beginning of the cooling stage.

Characterization. The bulk density of the sintered pellets was determined using Archimedes’ method, and the relative density was defined as the ratio between the experimental and the theoretical values. The theoretical density of materials was calculated with the rule of mixtures on the basis of the starting composition. Residual porosity, fibre volumetric content (FVC) and mean grain size (m.g.s) of ZrB_2 were measured by image analysis using the Image-Pro Analyzer 7.0 software (v.7, Media Cybernetics, USA) on SEM images of polished sections. The microstructures were analysed on polished and fractured surfaces using field emission scanning electron microscopy (FE-SEM, Carl Zeiss Sigma NTS Gmbh Öberkochen, Germany).

Four-point bending tests (σ) were performed on 25 × 2.5 × 2 mm^3 bars (length by width by thickness, respectively). Chevron notched beams (CNBs) specimens of 25 × 2 × 2.5 mm^3 (length by width by thickness, respectively) were used for toughness tests (K_I). The test bars were notched with a 0.1 mm-thick diamond saw; the chevron-notch tip depth and average side length were about 0.12 and 0.80 of the bar thickness, respectively. All tested bars were fractured using a semi-

articulated stainless steel four-point fixture with a lower span of 20 mm and an upper span of 10 mm, using a Zwick-Roell Z050 screw-driven load frame. The crosshead speed was 1 mm/min and 0.05 mm/min for σ and K_I, respectively. The Work-of-Fracture (WoF) was calculated from the CNB test as the area below the load-displacement curve divided by the double of the projected real surface.

3. Results and discussion

3.1 SPS vs HP - Microstructural features and fibre/matrix interface characteristics

Table 1 summarizes sintering conditions, densities and properties of the materials obtained.

Label	Sintering conditions				Sintering T_{onset}	Max densification rate	Density	Porosity	ZrB_2 mean grain size	Fibre volumetric content	Flexural strength, σ	Fracture toughness K_I
	(°C/min)	(°C)	(MPa)	(min)	(°C)	(%/min)	(g/cm^3)	(%)	(μm)	(%)	(MPa)	(MPa√m)
C_HP	25	1900	40	30	1600	0.9	3.0	18	~2.4	55	470 ± 50	10.0 ± 3.0
C_SPS	100	1850	40	3	1500	6	3.0	18	~2.3	55	300 ± 50	14.6 ± 3.0
U_HP	25	1900	40	30	1600	0.9	3.8	10	~2.5	45	320 ± 10	10.3 ± 0.3
U_SPS	100	1850	40	3	1500	6	4.0	5	~2.4	45	260 ± 20	8.7 ± 0.4

Table 1. Sintering parameters (heating rate, max temperature, pressure, residence time), physical properties and mechanical properties of specimens sintered by HP (C_HP, U_HP) and SPS (C_SPS, U_SPS) with coated PAN-derived fibres (C) and uncoated pitch-based fibres (U).

C_HP (reference sample): The composite with coated fibres, hot pressed at 1900 °C, showed a residual porosity of 18%, Table 1. Densification was aided by formation of Si-O liquid phases that helped particle rearrangement and favoured cleaning of the ZrB_2 particle surface from surficial ZrO_2 and B_2O_3, incorporating them in the liquid, as previously reported [30]. The typical densification curve is reported in Fig. 1a. The onset for densification was around 1600 °C, with a change in the slope related to an increase of the densification rate at around 1700 °C. The maximum

densification rate, ~0.9 % min^{-1}, was recorded during the heating step when temperature approached 1850 °C.

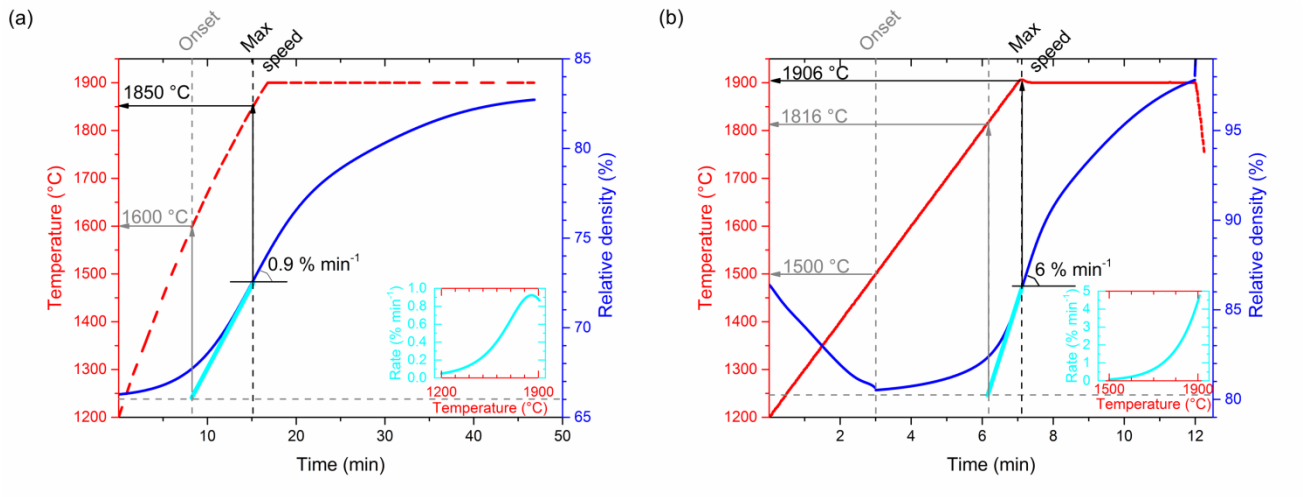

Fig. 1. Densification curves obtained for a) HP cycle at 1900 °C, 30 min, b) SPS cycle at 1900 °C, 5 min. In the inset the densification rate *vs.* temperature during heating step is shown.

Details of the microstructure, Fig. 2, show coated fibres grouped in clusters, Fig. 2a, with unaltered coating, Fig. 2b, c and isolated fibres with a reacted layer in place of the coating, at the interface, Fig. 2e. The coating was useful to prevent a strong fibre/matrix reaction, which would have been unavoidable in the case of uncoated fibres [25]. Around the fibres, we detected the formation of small bright contrasting grains and intermediate grey particles (Fig. 2c), which were recognized as ZrC and SiC particles by EDS (Fig. 2d). Formation of ZrC at the interface with C fibres was already reported in previous works [14] and is caused by carbo-reduction of ZrO_2 present on the surface of ZrB_2 particles with carbon provided by the fibres, see reaction 1.

$$ZrO_2 + 3C \rightarrow ZrC + 2CO \quad (1)$$

For isolated fibres, inclusions of ZrC and SiC particles inside the coating/fibres were detected and were due to penetration of Si-O based liquid phases inside the coating layers and subsequent reaction with the fibre, during sintering, see Fig 2e. The combination of unreacted

clustered coated fibres (Fig. 2b) and isolated fibres (Fig. 2e) with partially reacted interfaces led to a mixture of weak and strong interfaces, as depicted in the fracture image in Fig. 2f.

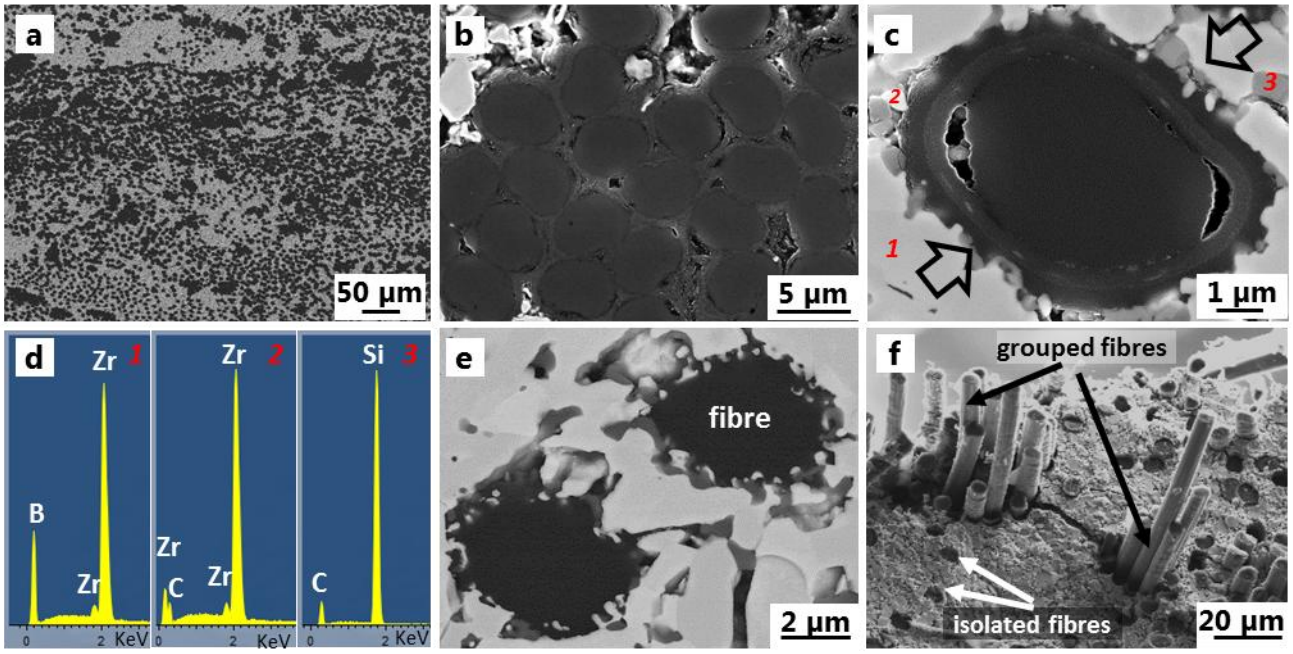

Fig. 2. Microstructural details of sample **C_HP**, a) polished cross section showing grouped fibres, b) magnification of the grouped fibres joined by the coating, c) coating detachment due to load application, d) EDS analysis of 3 different spots marked in fig. 2c as 1,2,3, e) two fibres with reacted coating, f) fracture surface with extensive pull-out of grouped fibres and no pull-out of isolated fibres.

C_SPS: Different trials were conducted to replicate similar microstructural features as for hot pressed samples. SPS cycles were first conducted at 1900 °C for 2, 3, 5 min, and then at 1850 °C for 2, 3, 5 min. The densification curve for the cycle at 1900 °C, 5 min, is reported in Fig. 1b. Besides the displacement originating from the thermal expansion effects of the pistons, the behaviour is similar to hot pressing. The onset of densification occurred roughly at 1500 °C; at 1800 °C a sudden increase of densification rate was observed. Due to the four times higher heating rate, the maximum value of densification rate, of about 6 % min^{-1}, was achieved after the heating step when the temperature reached the peak of 1906 °C. The higher densification rate for SPS compared to HP is likely due to the higher heating rate of the former. With these sintering conditions, full density was achieved; however, SEM analysis on the fracture surfaces revealed the degradation of

the fibre coating, leading to the loss of the coating functionality and no fibre debonding during fracture (Fig. 3). Decreasing the holding time from 5 to 2 minutes did not solve the issue of fibre/matrix overreaction, therefore it was necessary to decrease the maximum sintering temperature.

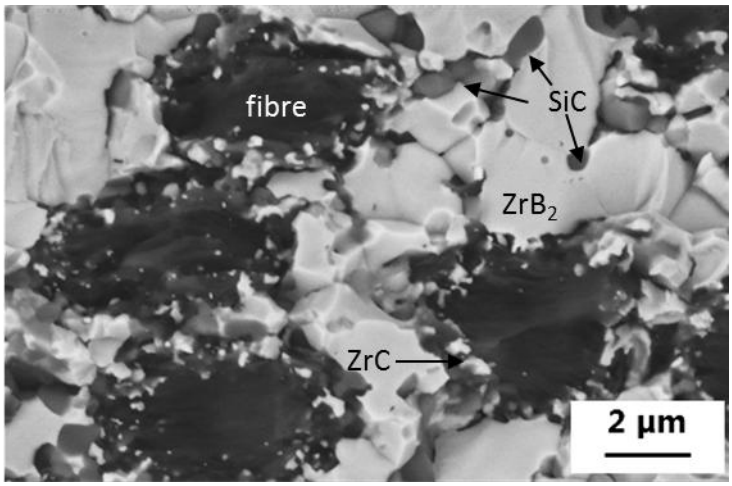

Fig. 3. Fracture surface of the damaged fibre highlighting a group of four fibre sections overreacted with the matrix. The dark contrasting rounded phases are the fibers, the light contrasting phase is the ZrB_2 matrix, the grey contrasting is SiC. The jagged interface containing ZrC particles is due to the overreaction of the fibre and matrix at the fibre/matrix interface during SPS at 1900 °C.

Cycles carried out at 1850 °C for shorter times, 2 min, were considered more suitable to achieve a level of densification (residual porosity < 20 %) in the matrix similar to the hot pressing one, with no fibre damage. A slight ZrB_2 grains refinement was observed for SPS, see Table 1.

Fig. 4 shows essential features of the composite sintered at 1850 °C for 2 min. Similar to C_HP the fibre distribution was uneven, due to the fibre coating applied before impregnation, see Fig. 4a. Indeed, the liquid slurry could not penetrate the bundles connected by the CVD PyC coating, and neither SPS nor HP did repair this defect. Noteworthy, inside fibre clusters a partial detachment of the coating from the fibre was frequently observed during densification (Fig. 4b). This detachment was likely due to shrinkage stresses occurring during the SPS treatment. On the contrary, isolated fibres showed a more reacted interface, and no coating detachment, see Fig. 4c, similar to hot pressing. Overall, the phenomenon of coating detachment was more marked after

SPS, Fig. 4b, very likely enhanced by the faster heating and cooling rate that did not allow a suitable rearrangement of particles inside the composites. On the other hand, the higher temperature and longer holding time of hot pressing caused a slightly higher reaction at the interface for isolated fibres, (compare Fig. 4c to 2e). In Fig. 4d a bimodal extensive fibre pull-out is visible, weak interface for grouped fibres and a strong interface for isolated fibres. Details in Fig. 4e, indicate that fibre sliding occurred predominantly between fibres and coating.

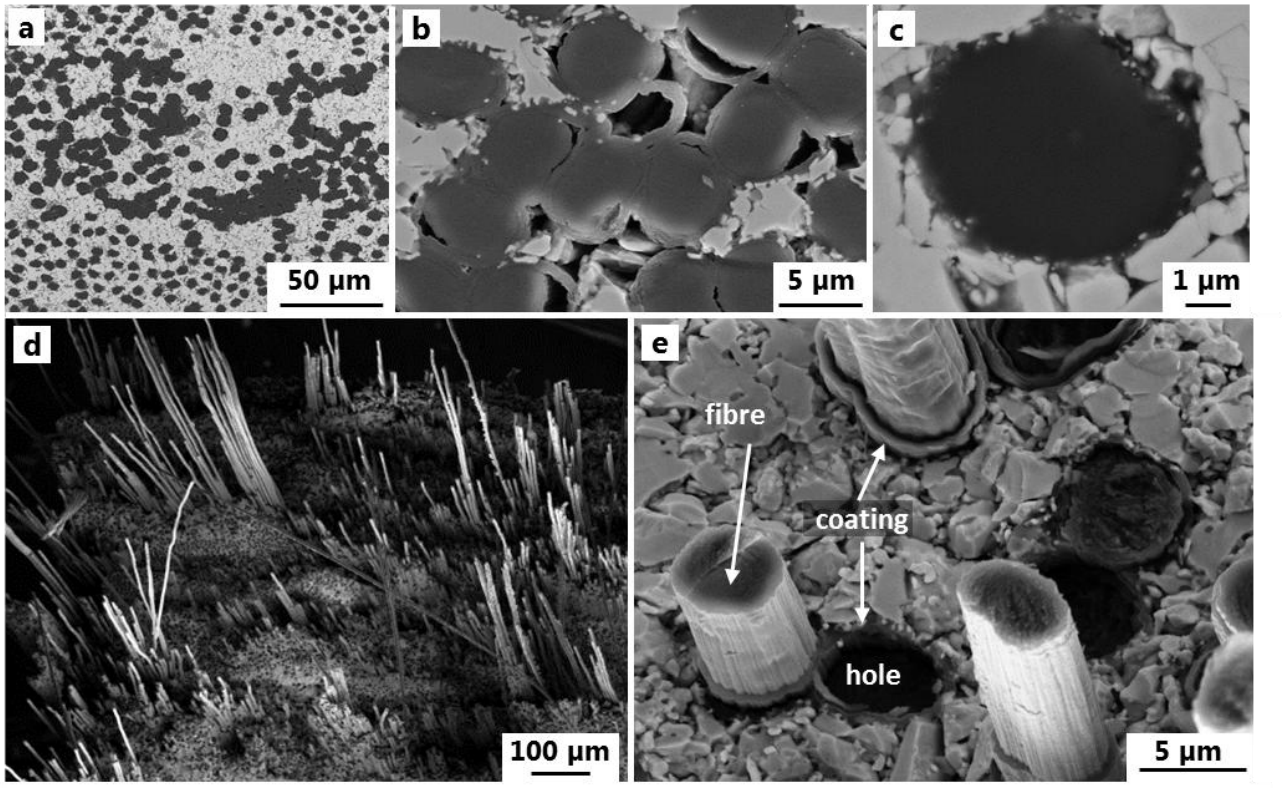

Fig. 4. Microstructural details of sample **C_SPS**, a) polished cross section showing grouped fibres, b) magnification of the grouped fibres showing coating detachment c) isolated fibre cross section with partially reacted coating, d) fracture surface with an extensive fibre pull-out, e) details of the interface after fibre sliding.

U_HP (reference HP sample): The microstructure obtained with uncoated pitch fibres is very different from the previous cases, Fig. 5a. This is due to several factors including the lower FVC, 45 vs 55 vol.% and a larger fibre diameter, ~10 µm. But most of all, uncoated fibres were more homogeneously infiltrated by the slurry compared to coated fibres (Fig. 5a,d). As for the matrix/fibre interface, it is clear that the absence of coating favoured a stronger adhesion with the

matrix (Fig. 5c), as previously reported [28], resulting in a decrease of fibre pull-out extent (Fig. 5d) compared to the samples with coated fibres (Fig. 2f). At the interface, the formation of SiC (Fig. 5c) and ZrC (not shown) was observed, as for the previous specimens.

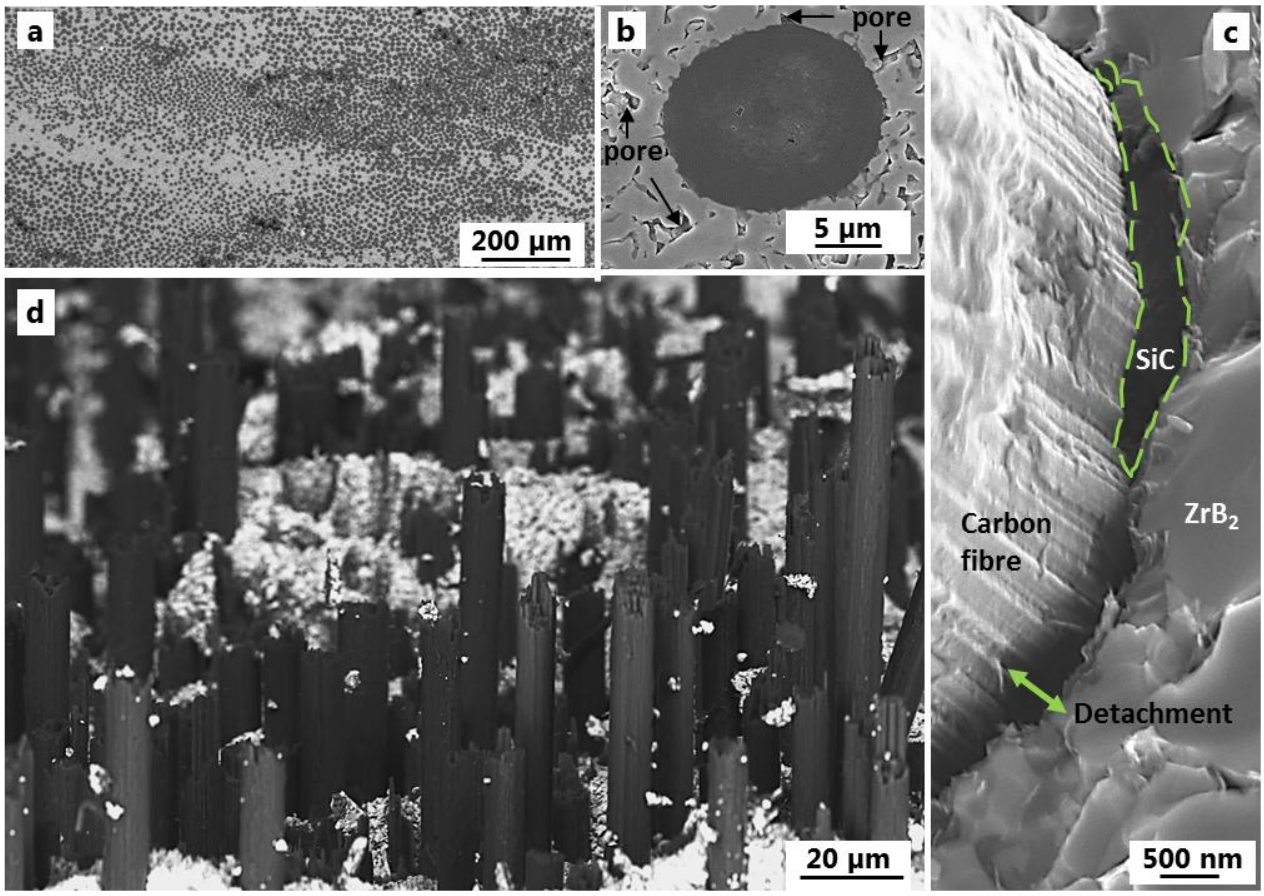

Fig. 5. Microstructural details of sample **U_HP**, a) polished cross section showing homogeneously distributed fibres in the matrix (dark contrasting are not infiltrated area), b) detail of a fibre cross section surrounded by the matrix (residual porosity highlighted by arrows), c) detail of fibre/matrix interface showing partial fibre detachment and partial matrix anchorage with residual SiC phase at the interface, d) fracture surface where fibre pull-out is visible, dark contrasting are fibres and white contrasting is matrix.

U_SPS: The composite was sintered at 1850 °C, 2 min, as for C_SPS. The final porosity was ~5% (Table 1), in agreement with microstructure analysis (Fig. 6a-b). As for U_HP, fibres are well distributed in the UHTC matrix and the interface was strong but quite smooth (Fig. 6c), just displaying small SiC particles. The extent of fibre pull-out was lower than the reference hot pressed sample, consisting with higher matrix density achieved, and occurred via intra-fibre sliding, Fig.

6d,e. Fig. 6e shows the external fibre graphite layer adherent to ZrB_2 matrix but detached from the rest of the fibre. The matrix mean grain size of U_HP and U_SPS are comparable, see Table 1.

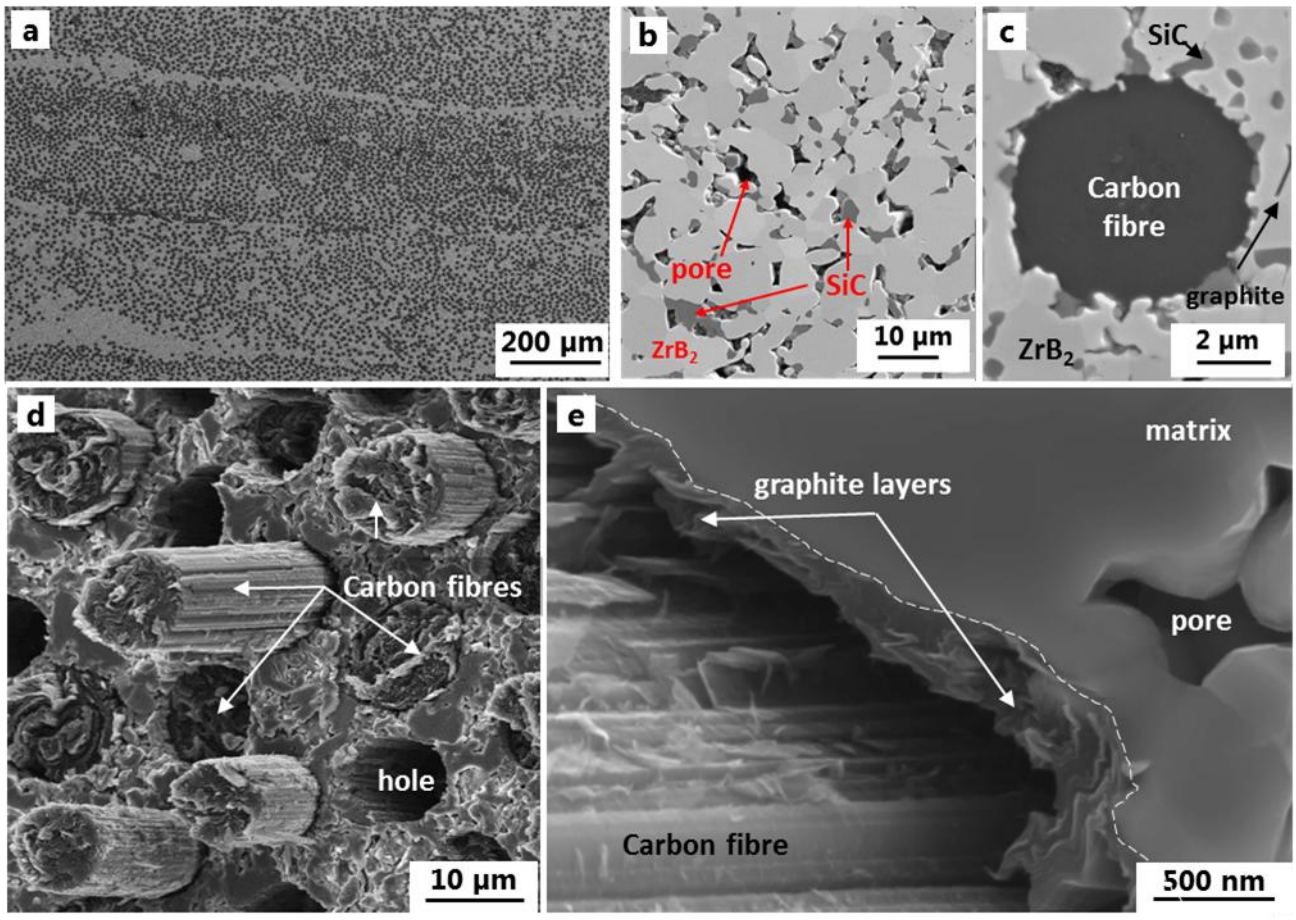

Fig. 6. Microstructural details of sample **U_SPS**, a) polished cross section showing well distributed fibres in the matrix, b) detail of the matrix, dark contrasting area are pores, the light contrasting phase is ZrB_2 matrix, the grey contrasting is SiC. c) single fibre polished section; d) fracture surface with short fibre pull-out, e) detail of fibre/matrix interface where graphite layers remained adherent to the matrix after intra-fibre sliding are visible.

In summary, experiments and microstructural analyses confirmed that it is possible to replicate the microstructure of a UHTCMC densified by hot pressing, using the SPS technique. The temperature must be lowered by some 50 °C and the holding time is reduced from half an hour to few minutes. This finding holds true for small and thin samples as those here considered but it is likely that experimental parameters must be re-adjusted in case of samples with different mass and dimensions. Parallel cycles at 1900 °C confirmed that SPS was much faster than hot pressing to

achieve nearly full density in the matrix, but the fibre/matrix interface reactivity was too high, which jeopardized the capability for damage tolerance of the composite. From the microstructural features and densification curves it was concluded that similar densification mechanisms occurred during the two thermal treatments, mostly based on conventional heating effects. For SPS, the Joule effect had the consequence of a faster heating compared to hot pressing and this accelerated the diffusion processes via liquid phase sintering. The presence of a coating allowed the use of PAN-derived fibres, previously found unsuitable for this process, by preventing the reaction at the interface between the fibre and the matrix. However, coated fibres were more delicate and the coating was prone to detachment during the sintering treatment very likely due to the application of a mechanical load. Pitch-based carbon fibres were suitable even without expensive coatings due to their higher chemical stability (graphitic structure), but the lack of a coating always resulted in a stronger fibre/matrix interface that limited fibre pull-out.

3.2 Mechanical behaviour

Flexural strength and fracture toughness load-displacement curves are reported in Fig. 7 and Fig. 8 respectively, highlighting the direct comparison between SPS and HP treatment on the same composition. For the sake of clarity, it must be mentioned that these tests were useful just for comparison purposes; it is well known that flexural strength values are affected by interlaminar fracture, thus it is unlikely that the values reported in Table 1 always represent the ultimate materials strength. The same holds true for fracture toughness, in which the reported value could be a mixture of opening mode (**mode I**) and shearing mode (**mode II**).

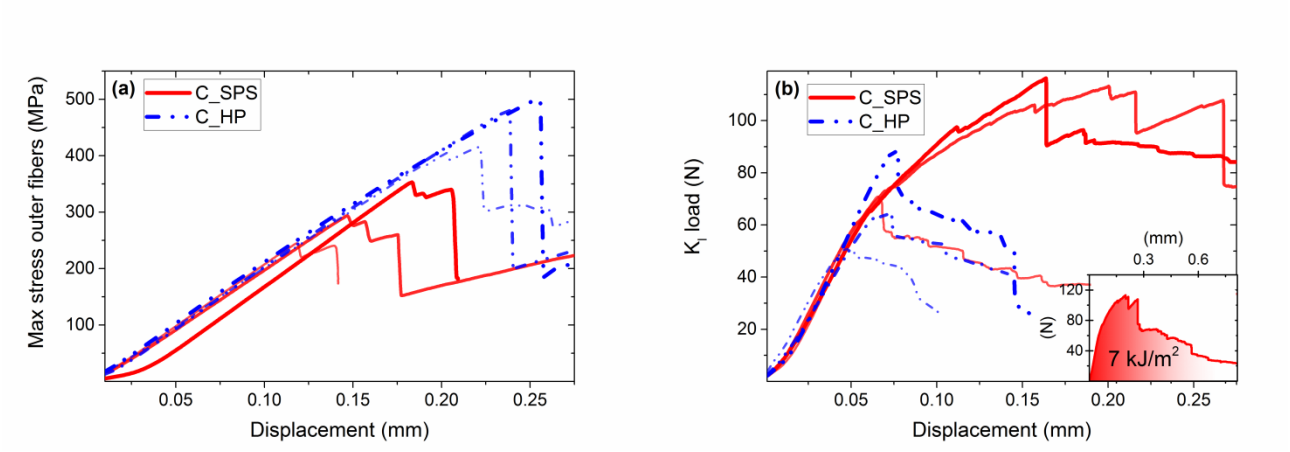

Fig. 7. C_SPS vs C_HP: a) Comparison of stress-displacement curves of the flexural test and b) load-displacement curves of chevron notched beams (CNB) specimens.

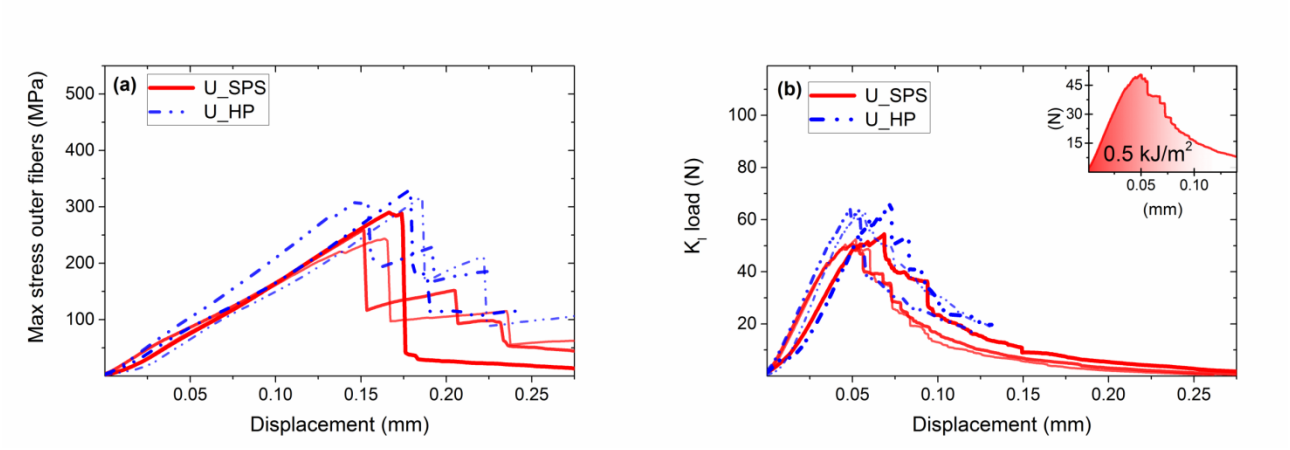

Fig. 8. U_SPS vs U_HP: Comparison of stress-displacement curves of the flexural test and b) load-displacement curves of chevron notched beams (CNB) specimens for samples.

C_SPS vs C_HP. The results obtained in terms of mechanical strength and toughness can be easily interpreted on the basis of the microstructural observations. Comparing samples C_SPS and C_HP, coated fibres and different techniques, Fig. 7, a lower strength was found when SPS was the sintering technique, Fig. 7a, while the toughness was improved up to a corresponding Work-of-Fracture (WoF) of 7 KJ/m^2, Fig. 7b. Stresses induced by a rapid densification, fast heating and cooling led to creation of new defects, such as coating detachment, lower adhesion between layers compared to HP, because powder particles inside and around impregnated bundles had less time for rearrangement. This probably resulted in a higher chance of interlaminar fracture and crack growth

in **mode II**. On the other hand, the rapid heat treatment limited the fibre/matrix interface reactions, leading to higher fracture toughness.

U_SPS vs U_HP. For this group of composites, the difference recorded in mechanical properties between the two techniques is much less evident and the WOF is attested to about 0.5 KJ/m^2, Fig. 8a, b. The slightly lower values of toughness found for U_SPS can be attributed to the stronger fibre/matrix bond. The load-displacement curves of CNBs, Fig. 8b, showed a similar trend and could be affected by a lower contribution of crack growth in **mode II**. Also the lower data scattering of both mechanical tests suggests that a more homogeneous microstructure was obtained with uncoated pitch-based carbon fibres.

As a general observation ultra-high modulus pitch-based carbon fibres show a lower degree of reaction during sintering with oxide impurities, SiC and ZrB_2 grains compared to intermediate modulus PAN-derived fibres. The reason lies in the different microstructure of the carbon, which is highly crystalline with a graphitic structure for the former, and amorphous with a turbostractic structure for the latter. Such difference in structure is responsible for the intra-fibre-sliding in pitch-based C_f and, at the same time, the unsuitability of uncoated PAN-based C_f [25]. About the lower delamination and the higher microstructure homogeneity of the material reinforced with uncoated pitch-based fibres, a possible explanation, could be the faster rearrangement during sintering under uniaxial pressure, of isolated C_f rather than joined grouped C_f.

Flexural strength and toughness were higher in composites with coated PAN-based fibres. This could be associated to both the higher FVC and the intrinsically higher strength of the PAN-derived fibres which was retained even after sintering. Compared to pitch-based carbon fibres [26], coated PyC/PAN-based carbon fibres allowed for an extensive fibre pull-out from the UHTC matrix upon fracture. The coating was well anchored to the matrix, but the fibre/coating interface remained weak and fibres were able to slide out of the coating. Moreover, the lower stiffness of the PAN-derived fibres prevented premature fibre failure during sliding.

As far as the fracture toughness of hot pressed specimens is concerned, the individual values of K_I did not highlight any significant difference between coated and uncoated fibres. The apparently higher mean values, obtained with the coated C_f, should be addressed to the higher tendency to delaminate, which on the one side attests the higher damage tolerance behaviour. On the other side, owing the higher contribution of shearing mode, the calculated K_I values are not reliable as absolute values.

4. Conclusions

In this paper, for the first time, the feasibility of SPS for the consolidation of continuous fibre reinforced ZrB_2-SiC composites was demonstrated. Specimens reinforced with both coated PAN-based fibres or pitch-derived carbon fibres were successfully sintered by SPS and it was shown that microstructure and mechanical properties were comparable to materials produced by hot pressing.

Consolidation by SPS was much faster, but required a fine tuning of the sintering parameters to limit excessive reaction at fibre/matrix interface. Comparison of shrinkage curves and microstructures indicated that C_f/ZrB_2-SiC sintered by HP and SPS underwent similar densification mechanisms, e.g. liquid phase sintering, and similar chemical interactions between the involved species. Spark plasma sintered composites reinforced with 55 vol% of coated fibres reached a strength of 300 MPa and a fracture toughness of 15 MPa√m.

Acknowledgements

This work received support by the European Union's Horizon 2020 research and innovation programme under Grant Agreement n°685594. (C^3HARME: Next Generation Ceramic Composites for Harsh Combustion Environment and Space). Authors gratefully acknowledge A. Schoberth (AIRBUS group) for supplying coated fibres, C. Melandri and D. Dalle Fabbriche, CNR-ISTEC for technical support.

References

[1] Z.A. Munir, U. Anselmi-Tamburini, M. Ohyanagi, The effect of electric field and pressure on the synthesis and consolidation of materials: A review of the spark plasma sintering method, J. Mater. Sci. 41 (2006) 763–777. doi:10.1007/s10853-006-6555-2.

[2] R. Orrù, G. Cao, Comparison of reactive and non-reactive spark plasma sintering routes for the fabrication of monolithic and composite Ultra High Temperature Ceramics (UHTC) materials, Materials (Basel). 6 (2013) 1566–1583. doi:10.3390/ma6051566.

[3] G. Cao, C. Estournes, J. Garay, R. Orru, eds., Spark Plasma Sintering, 1st Ed., Elsevier, 2019. doi:https://doi.org/10.1016/C2018-0-02428-7.

[4] J. Lin, Y. Huang, H. Zhang, Y. Yang, Y. Wu, Spark plasma sintering of ZrO2 fiber toughened ZrB2-based ultra-high temperature ceramics, Ceram. Int. 41 (2015) 10336–10340. doi:10.1016/j.ceramint.2015.04.148.

[5] H. Hu, Q. Wang, Z. Chen, C. Zhang, Y. Zhang, J. Wang, Preparation and characterization of C/SiC–ZrB2 composites by precursor infiltration and pyrolysis process, Ceram. Int. 36 (2010) 1011–1016. doi:https://doi.org/10.1016/j.ceramint.2009.11.015.

[6] C. Xu, Y. Cai, K. Flodström, Z. Li, S. Esmaeilzadeh, G. Zhang, Spark plasma sintering of B4C ceramics : The effects of milling medium and TiB2 addition, Int . J. Refract. Met. Hard Mater. 30 (2012) 139–144. doi:10.1016/j.ijrmhm.2011.07.016.

[7] H. Jin, S. Meng, W. Xie, C. Xu, J. Niu, ZrB2-CNTs Nanocomposites Fabricated by Spark Plasma Sintering, Materials (Basel). 9 (2016) 967. doi:10.3390/ma9120967.

[8] X. Zhang, L. Xu, S. Du, C. Liu, J. Han, W. Han, Spark plasma sintering and hot pressing of ZrB2-SiCW ultra-high temperature ceramics, J. Alloys Compd. (2008). doi:10.1016/j.jallcom.2007.11.018.

[9] J. Gonzalez-Julian, K. Jähnert, K. Speer, L. Liu, J. Räthel, M. Knapp, H. Ehrenberg, M. Bram, O. Guillon, Effect of Internal Current Flow during the Sintering of Zirconium Diboride by Field Assisted Sintering Technology, J. Am. Ceram. Soc. 99 (2016) 35–42. doi:10.1111/jace.13931.

[10] G.B. Yadhukulakrishnan, S. Karumuri, A. Rahman, R.P. Singh, A. Kaan Kalkan, S.P. Harimkar, Spark plasma sintering of graphene reinforced zirconium diboride ultra-high temperature ceramic composites, Ceram. Int. 39 (2013) 6637–6646. doi:10.1016/j.ceramint.2013.01.101.

[11] E. Zapata-Solvas, D.D. Jayaseelan, H.T. Lin, P. Brown, W.E. Lee, Mechanical properties of ZrB2- and HfB2-based ultra-high temperature ceramics fabricated by spark plasma sintering,

J. Eur. Ceram. Soc. 33 (2013) 1373–1386. doi:10.1016/j.jeurceramsoc.2012.12.009.

[12] J. Zou, J. Liu, J. Zhao, G.J. Zhang, S. Huang, B. Qian, J. Vleugels, O. Van der Biest, J.Z. Shen, A top-down approach to densify ZrB2-SiC-BN composites with deeper homogeneity and improved reliability, Chem. Eng. J. (2014). doi:10.1016/j.cej.2014.03.089.

[13] S.-Q. Guo, Densification of ZrB2-based composites and their mechanical and physical properties: A review, J. Eur. Ceram. Soc. 29 (2009) 995–1011. doi:10.1016/j.jeurceramsoc.2008.11.008.

[14] L. Zoli, A. Vinci, L. Silvestroni, D. Sciti, M. Reece, S. Grasso, Rapid spark plasma sintering to produce dense UHTCs reinforced with undamaged carbon fibres, Mater. Des. 130 (2017) 1–7. doi:10.1016/j.matdes.2017.05.029.

[15] R. Savino, L. Criscuolo, G.D. Di Martino, S. Mungiguerra, Aero-thermo-chemical characterization of ultra-high-temperature ceramics for aerospace applications, J. Eur. Ceram. Soc. 38 (2018) 2937–2953. doi:10.1016/j.jeurceramsoc.2017.12.043.

[16] W. Krenkel, Ceramic Matrix Composites: Fiber Reinforced Ceramics and their Applications, 2008. doi:10.1002/9783527622412.

[17] M.E. Westwood, J.D. Webster, R.J. Day, F.H. Hayes, R. Taylor, Review Oxidation protection for carbon fibre composites, J. Mater. Sci. 31 (1996) 1389–1397. doi:10.1016/0008-6223(89)90204-2.

[18] A. Vinci, L. Zoli, E. Landi, D. Sciti, Oxidation behaviour of a continuous carbon fibre reinforced ZrB2–SiC composite, Corros. Sci. 123 (2017). doi:10.1016/j.corsci.2017.04.012.

[19] S. Tang, J. Deng, S. Wang, W. Liu, K. Yang, Ablation behaviors of ultra-high temperature ceramic composites, Mater. Sci. Eng. A. 465 (2007) 1–7. doi:10.1016/j.msea.2007.02.040.

[20] A. Paul, J. Binner, B. Vaidhyanathan, UHTC Composites for Hypersonic Applications, in: Ultra-High Temp. Ceram. Mater. Extrem. Environ. Appl., 2014: pp. 144–166. doi:10.1002/9781118700853.ch7.

[21] J.W. Zimmermann, G.E. Hilmas, W.G. Fahrenholtz, Thermal shock resistance of ZrB2 and ZrB2-30% SiC, Mater. Chem. Phys. 112 (2008) 140–145. doi:10.1016/j.matchemphys.2008.05.048.

[22] B. Xu, C. Hong, S. Zhou, J. Han, X. Zhang, High-temperature erosion resistance of ZrB2-based ceramic coating for lightweight carbon/carbon composites under simulated atmospheric re-entry conditions by high frequency plasma wind tunnel test, Ceram. Int. 42 (2016) 9511–9518. doi:http://dx.doi.org/10.1016/j.ceramint.2016.03.029.

[23] Q. Li, S. Dong, Z. Wang, G. Shi, Fabrication and properties of 3-D Cf/ZrB2-ZrC-SiC composites via polymer infiltration and pyrolysis, Ceram. Int. 39 (2013) 5937–5941.

doi:10.1016/j.ceramint.2012.11.074.

[24] S. Tang, J. Deng, S. Wang, W. Liu, Comparison of thermal and ablation behaviors of C/SiC composites and C/ZrB2-SiC composites, Corros. Sci. 51 (2009) 54–61. doi:10.1016/j.corsci.2008.09.037.

[25] D. Sciti, A. Natali Murri, V. Medri, L. Zoli, Continuous C fibre composites with a porous ZrB2 Matrix, Mater. Des. 85 (2015). doi:10.1016/j.matdes.2015.06.136.

[26] L. Zoli, A. Vinci, P. Galizia, C. Melandri, Di. Sciti, On the thermal shock resistance and mechanical properties of novel unidirectional UHTCMCs for extreme environments, Sci. Rep. (2018). doi:10.1038/s41598-018-27328-x.

[27] V. Rubio, P. Ramanujam, J. Binner, Ultra-high temperature ceramic composite, Adv. Appl. Ceram. (2018). doi:10.1080/17436753.2018.1475140.

[28] P. Galizia, S. Failla, L. Zoli, D. Sciti, Tough salami-inspired Cf/ZrB2 UHTCMCs produced by electrophoretic deposition, J. Eur. Ceram. Soc. 38 (2018) 403–409. doi:10.1016/J.JEURCERAMSOC.2017.09.047.

[29] S. Mungiguerra, G.D. Di Martino, A. Cecere, R. Savino, L. Silvestroni, A. Vinci, L. Zoli, D. Sciti, Arc-jet wind tunnel characterization of ultra-high-temperature ceramic matrix composites, Corros. Sci. (2019). doi:https://doi.org/10.1016/j.corsci.2018.12.039.

[30] W.G. Fahrenholtz, G.E. Hilmas, I.G. Talmy, J.A. Zaykoski, Refractory diborides of zirconium and hafnium, J. Am. Ceram. Soc. 90 (2007) 1347–1364. doi:10.1111/j.1551-2916.2007.01583.x.